Styrene synthesis: in situ characterization and reactivity studies of unpromoted and potassium-promoted iron oxide model catalysts

Osama Shekhah, Wolfgang Ranke,* and Robert Schlögl

Department of Inorganic Chemistry, Fritz Haber Institute of the MPG, Faradayweg 4-6, 14195 Berlin, Germany

Received 19 December 2003; revised 15 March 2004; accepted 15 March 2004

Available online 24 April 2004

Abstract

Styrene synthesis over iron oxide model catalysts was studied by combining UHV characterization methods with in situ conversion measurements in a microflow reactor under realistic reaction conditions. Both unpromoted Fe_2O_3 and K-promoted model catalysts show a similar high starting activity while that of Fe_3O_4 is clearly lower. Water limits and K promotion slows down deactivation by coking and oxide reduction. The deactivation can be prevented and the high initial yield preserved by adding a small amount of oxygen to the feed. Both the presence of Fe^{3+} and intermediate adsorption strength for ethylbenzene and styrene are essential for high conversion yields.
© 2004 Elsevier Inc. All rights reserved.

Keywords: Carbonaceous deposits; Dehydrogenation; Deactivation; Ethylbenzene; Iron oxide; Oxygen; Potassium; Promoter; Styrene; Water

1. Introduction

The dehydrogenation of ethylbenzene (EB) to styrene (St) [1] is one of the 10 most important organic catalytic processes by which presently more than 23 million tons of St are produced per year [2]. The dehydrogenation occurs at ~ 870 K in the presence of overheated steam over iron oxide-based catalysts:

$$C_8H_{10} \rightarrow C_8H_8 + H_2. \tag{1}$$

The main precursors of the technical catalyst are hematite (Fe_2O_3) and the promoter potassium carbonate (K_2CO_3) which are mixed and calcined. Small amounts of other metal oxides like Cr_2O_3 are added as structural promoters to stabilize the catalyst morphology and prevent sintering. Promotion of iron oxide with potassium enhances the reactivity of iron oxide by an order of magnitude and reduces the formation of carbonaceous surface deposits (here shortly called coke) that deactivate the catalysts [1,3–5].

In order to understand the kinetics of the dehydrogenation reaction [4,6] the catalyst function and the deactivation process [7–9], many studies have been carried out on the technical catalyst. A study on the catalyst structure and composition under reaction conditions by Muhler et al. [7,8] gave

evidence for the existence of $KFeO_2$ which, in line with a proposal of Hirano [5], was interpreted as essential for high activity. Kinetic studies on model catalysts at pressures in the mbar range showed similar apparent activation energies for potassium promoted and unpromoted iron oxide catalysts. It was therefore proposed that potassium only increases the number of active sites, but does not change their nature [6]. Potassium stabilizes the catalyst against reduction [10] and supports the removal of coke. K_2CO_3 is believed to represent the active center for carbon gasification [5,11,12]. Benzene and toluene as the main side products may be formed at different sites [5,6,13]. Experiments on unpromoted Fe_2O_3 in the low- and medium-pressure range gave clear evidence that defective surfaces are more active than well-ordered ones [14,15].

The reaction is run in presence of overheated steam in excess, which is believed to remove coke that deactivates the catalyst, to supply heat for the endothermic dehydrogenation reaction ($\Delta H = 124$ kJ mol^{-1}), to prevent reduction of the oxide catalyst, and to act as a diluent in order to shift the reaction equilibrium toward the product side [3].

The catalyst deactivates slowly and needs to be replaced after about 2 years. Since this is a costly process, the deactivation was studied extensively. The main reasons for deactivation are coke deposition, which was found to be higher in the case of the unpromoted catalyst, loss or redistribution of the potassium promoter during reaction, reduction of

the catalyst by the hydrogen formed during the reaction and physical degradation of the catalyst [9,16].

All attempts to prevent the complex deactivation process [17] have concentrated on developing the catalyst material by adding more promoters or by supporting the catalyst in order to improve its performance. Comparatively little is known about the reaction mechanism on an atomic scale, about the chemical transformations which happen during the reaction, or about the real active phase during reaction.

Our approach is to bridge the pressure and material gap between reactivity studies in ultrahigh vacuum (UHV) and real catalysis by combining surface science methods for model catalyst characterization [18] with in situ activity measurements under realistic reaction conditions. Using a stagnation point microflow reactor [19] and pre- and postreaction surface analysis, we try to understand the structure, the composition-reactivity correlations, and the chemical transformations which occur under the course of reaction.

In this work we present investigations on the dehydrogenation reaction of EB to St, first over single crystalline iron oxide model catalyst films of the composition $Fe_3O_4(111)$ and α-$Fe_2O_3(0001)$, then over promoted films of the general composition KFe_xO_y with different potassium content and x, y adjusting correspondingly. The reactions were performed under near-technical process conditions with different feed compositions.

2. Experimental

2.1. Instrumentation

The experiments are performed in an UHV chamber with a base pressure of 10^{-10} mbar. It contains standard facilities for sample cleaning and is equipped with a back-view display optics for low-energy electron diffraction (LEED), a cylindrical mirror analyzer for Auger electron spectroscopy (AES) measurements, and a mass spectrometer. High pressure oxidation treatment and reaction experiments are performed in a preparation cell, which can be separated from the analysis chamber by a gate valve after sample transfer. Using a laser heating system [19], up to 1100 K can be reached in 1 mbar oxygen and up to 900 K in a flow of He at 1 bar. Temperature-programmed oxidation (TPO) experiments were performed after reaction experiments by transferring the sample back to the analysis chamber and heating to 1000 K in 10^{-6} mbar oxygen. TPO removes carbon deposits from the sample [14] but reoxidation, although thermodynamically favored, is kinetically hindered and does not occur even within extended periods at this low oxygen pressure [20].

2.2. Preparation of model catalyst thin films

A clean Pt(111) surface is prepared by cycles of argon ion bombardment (1 keV) and annealing to 1300 K. Iron is

evaporated onto this surface by resistively heating a tungsten wire with an iron wire wrapped around it. As described in more detail in [18], 10–20 nm thick $Fe_3O_4(111)$ films are prepared by repeated cycles of iron deposition at room temperature and subsequent oxidation for about 10 min at 950 K in 5×10^{-7} mbar oxygen partial pressure. $Fe_3O_4(111)$ is transformed into α-$Fe_2O_3(0001)$ films by oxidation for 15 min at oxygen pressures above 0.1 mbar at 1050 K. The different phases of iron oxide exhibit different LEED patterns, which makes it easy to distinguish them and to check that single-phased films were prepared. The sharpness of LEED spots and the background serve as a qualitative measure for surface domain size and defect density. However, even surfaces yielding sharp spots and low background usually still contain defects which cannot be analyzed using a simple display LEED optics.

Promoted iron oxide thin films (KFe_xO_y) are prepared by deposition of potassium at room temperature from an SAES getter source on the $Fe_3O_4(111)$ or $Fe_2O_3(0001)$ iron oxide thin films, followed by annealing up to 950 K in vacuum or in 1×10^{-6} mbar oxygen. For high potassium contents, deposition-annealing or deposition-oxidation cycles were repeated and the annealing temperature was lowered. A measure for the near-surface concentration of potassium is the Auger peak intensity ratio I_K/I_{Fe}. Most films are well ordered. Usually, LEED shows the periodicity of the close-packed oxygen layers in the film (see, e.g., the pattern before reaction in Table 3, A, which we call quasi-1 × 1-structure) which is half that of the surface periodicity of $Fe_3O_4(111)$. This means that the arrangement of the surface iron atoms which in Fe_3O_4 determine the surface periodicity is distorted and has no long-range order. Only for one special composition, a long-range ordered phase with a 2 × 2 super-structure with respect to the surface structure of $Fe_3O_4(111)$ is observed. It was assigned to a K-β''-ferrite-type film $K_xFe_{22}O_{34}(0001)$ ($x \approx 0.67$) [21–23]. In the Auger spectrometer used here, its Auger intensity ratio is $I_K/I_{Fe} = 2.7$. Films with higher K content ($I_K/I_{Fe} > 3$) have no long-range order. LEED shows no spots and a high background intensity. According to [22,23], such films are covered by a disordered $KFeO_2$ layer.

2.3. The reactor

Fig. 1 shows the used microflow reactor [19]. It is constructed on a 70-mm o.d. flange which carries the feedthroughs for the thermocouple and for two fiber rods which are used for coupling in laser radiation for sample heating. Two flexible capillaries are connected to the reactor cap, one for admission of the reactant gas mixture and one as product gas outlet. When the reactor cap is retracted, the sample on a sapphire support can be inserted. When the cap is closed, the arrangement represents a stagnation point reactor with a total volume of only about 4 ml. Due to the small distance between sample and cap (typically 1 mm), the gas volume in contact with the sample is
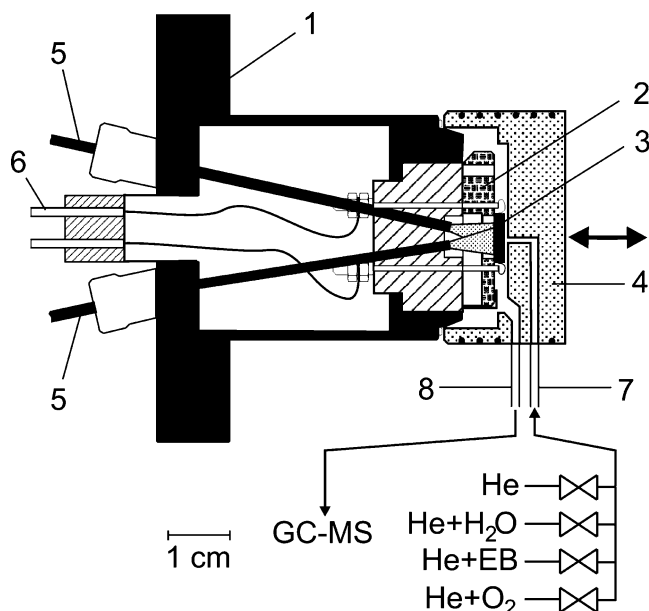
Fig. 1. Single-crystal flow reactor, schematically. (1) Reactor body, (2) sapphire sample support, (3) sample, (4) retractable reactor cap, (5) coupling for laser radiation, (6) thermocouple feedthrough, (7) flexible capillary for reactant gases, (8) flexible capillary for product gases.

Table 1
Partial pressures and molar ratios of reactive gases in the gas feed for the used standard reaction conditions [a]

Reaction conditions	p (mbar)	Molar ratios
Normal	$p(EB) = 3.3$ $p(H_2O) = 33$	$EB:H_2O$ 1:10
Reductive	$p(EB) = 3.3$	–
Oxidative	$p(EB) = 3.3$ $p(H_2O) = 33$ $p(O_2) = 1.7$	$EB:H_2O:O_2$ 1:10:0.5

[a] The rest to the working pressure of 1 bar is He. The standard reaction temperature is 870 K, the standard total flow 25 ml min^{-1}.

11. Postreaction characterization by AES, LEED; if necessary removal of coke by TPO cycle(s), followed by AES and LEED.

In order to make sure that the catalytic reaction really starts on the surface as characterized before in UHV, the conditions during sample heating (step 5) which takes about 20 min were considered carefully. Fe_2O_3 samples which were oxidized before in $p(O_2) > 0.1$ mbar were heated in an atmosphere of $He:H_2O:O_2 \approx 38:1.6:1$ (molar ratios) at a total flow rate of about 20 ml min^{-1}. Fe_3O_4 was heated with only H_2O in the He flow since it turned out that water prevents further reduction of Fe_3O_4. KFe_xO_y samples were heated in a He flow without any admixture. Back-transfer of a Fe_2O_3 sample after this heat up and cool down without reaction showed that the surface was still clean and showed the characteristic LEED pattern. During cool down after the reaction (step 9), the flow of He was maintained until T was below 500 K. Heating up again a sample in He after cool down and restarting the reaction showed the same catalytic activity as before cool down. The standard reaction conditions are listed in Table 1.

The measured quantities are GC peak areas. Under typical reaction conditions, the sum of the peak areas of all aromatics (EB, St and sometimes traces of toluene, benzene) is $\sim 95\%$ of the EB peak area without reaction (e.g., at low temperature). The missing $\sim 5\%$ go thus into products which we cannot detect like C_xH_y, CO, CO_2, and H_2. The highest observed conversions were $\sim 10\%$ so that the EB peak area corresponds in all cases to more than about 85% of the admitted EB. In view of the uncertainties of the EB flux and the sample area which enter the determination of an absolute rate, we neglect the missing 15% and refer the conversion yield y in percentage to the main EB peak area as measured. The conversion rates presented below are then calculated from the yield according to

$$r \, (cm^{-2} \, s^{-1}) = \left[F \times y \, (\%) \times 10^2 \right] / A = 6.54 \times 10^{14} y \, (\%), \tag{2}$$

with the EB flux $F = 3.27 \times 10^{16}$ molecules s^{-1} and the model catalyst area $A = 0.5$ cm^2. Rates are always given in St molecules cm^{-2} s^{-1}.
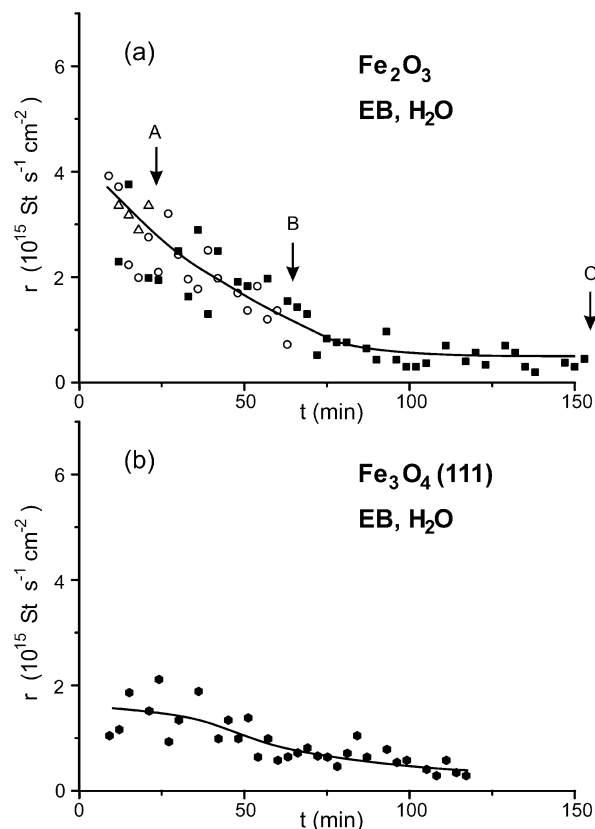
much smaller (~ 0.05 ml). Under typical flow conditions ($p = 1$ bar, 25 ml min^{-1}), the contact time is about 0.12 s.

The sample is heated from behind by radiation from two diode laser stacks with a total power of maximum 100 W, which is necessary to reach a reaction temperature of 870 K under flow conditions. EB and H_2O flow is achieved by conducting He carrier gas through saturators at 303 K. O_2 is admitted from a 20% O_2 in He gas supply. Product analysis is performed every 3 min with a gas chromatograph equipped with an ion-trap mass analyzer (GC-MS). The used setup is optimized for separation and analysis of EB, St, toluene, and benzene but not suitable for smaller hydrocarbons, for CO_2, CO and H_2.

The standard reaction experiment consists of the following steps:

1. Sample preparation in UHV, pre-reaction characterization by LEED and AES,
2. Sample transfer under vacuum into the reactor,
3. Preheating the reactor cap to 400 K and outgassing in vacuum,
4. Backfilling the reactor chamber with N_2 ($p = 1$ bar),
5. Sample heating during flow of He, if wanted with admixture of H_2O and/or O_2,
6. After reaching the T_{reac}: H_2O and/or O_2 are stopped (if wanted), EB is admitted, GC-MS is started,
7. Reactivity measurement at 870 K, EB in He, if wanted with admixture of H_2O and/or O_2,
8. Stop of EB, H_2O, O_2,
9. Cooling in He to $T < 500$ K,
10. Evacuation and back-transfer to UHV,

Fig. 2. Time dependence of the St conversion rate at 870 K, normal conditions, EB and H_2O in the feed, over (a) α-Fe_2O_3(0001) and (b) Fe_3O_4. The labels A–C give the positions where sample characterization was performed (see Table 2).

The oxide films are completely closed but on the side of the sample along its circumference, uncovered Pt might exist. Although Pt effectively dehydrogenates EB, it does not contribute to St production. It was shown [24] that St is bound so strongly that it does not desorb. Already at 400 K, adsorbed St polymerizes, followed by dehydrogenation. Beyond $\sim$ 700 K, it is completely dehydrogenated and a closed coke film with essentially graphitic properties has formed.

The conversion rate on a sample incidentally contaminated by SiO_2 was below $\sim 0.1 \times 10^{15}$ cm^{-2} s^{-1}, which is the detection limit of our GC. This represents the upper limit of the blind activity of the reactor.

3. Results

3.1. Unpromoted model catalyst

3.1.1. Dehydrogenation on α-Fe_2O_3(0001) and Fe_3O_4(111) in presence of steam

Fig. 2a shows that the initial conversion rate for St produced from EB dehydrogenation on the unpromoted catalyst Fe_2O_3 is relatively high $\sim 4 \times 10^{15}$, and drops within $\sim$ 70 min to a final rate of $\sim 0.5 \times 10^{15}$. Post reaction characterization using AES reveals relatively strong coke depo-

sition, $I_C/I_{Fe} = 3.4$ (C in Table 2). After TPO, LEED shows that the oxide is reduced to Fe_3O_4. For one sample, an ex situ surface analysis (transfer in air) by scanning tunneling microscopy (STM) was performed after reaction without a preceding TPO cycle. The corrugation over a distance of 500 nm had increased from typically 5 nm (clean surface) to about 15 nm (after reaction) which, however, still represents a quite smooth surface.

The reaction was repeated twice on a freshly prepared catalyst and was interrupted after different periods. In the high rate region (A in Fig. 2a and Table 2) the catalyst is covered by a small amount of coke $I_C/I_{Fe} = 1.1$ and the ratio I_O/I_{Fe} has decreased. After one TPO cycle, LEED shows that the catalyst still consists of Fe_2O_3 but the spots are more diffuse and the background is more intense. After 50 min (B in Fig. 2a and Table 2) the carbon deposits have increased $I_C/I_{Fe} = 3.6$. Three TPO cycles are necessary to remove them. Then the surface exhibits overlapping LEED patterns of both Fe_2O_3 and Fe_3O_4. We believe that the near-surface region of the catalyst had been reduced to disordered Fe_3O_4, while reordering and phase separation into Fe_2O_3 and Fe_3O_4 domains occurred during the TPO experiments which include heating. The deactivation is thus related either to carbon deposition or to reduction of the surface layer to Fe_3O_4 to a depth determined by oxygen diffusion or to both.

Fig. 2b shows that the initial conversion on the unpromoted Fe_3O_4 catalyst is lower, $\sim 1.5 \times 10^{15}$. Within about 45 min it deactivates to the same final rate as in Fig. 2a and is coked, $I_C/I_{Fe} = 5.0$. LEED after TPO shows that the surface still exhibits the Fe_3O_4 pattern, but also here the spots are weaker and the background is stronger, indicating an increased defect concentration (D in Table 2). The final state is the same as when starting with Fe_2O_3. In both cases, there is an increase in the intensity ratio I_O/I_{Fe} which we attribute to the presence of some oxygen in the carbon deposits on the catalyst surface. Since the final activity is the same on a completely coked sample (see next section), we believe that it represents the activity of carbon deposits on the catalyst surface.
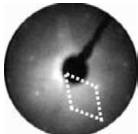
These results show that the high starting activity in Fig. 2a is related to clean Fe_2O_3 which exhibits a higher activity than Fe_3O_4. Assuming a site density of 2.3×10^{14} cm^{-2}, the density of surface unit cells on Fe_2O_3, the turnover frequency TOF for the initial high rate ($\sim 4 \times 10^{15}$) is ~ 10 St molecules per site and per second which is a reasonable value for a good catalyst.

3.1.2. Dehydrogenation on α-Fe_2O_3(0001) without steam

Fig. 3 shows the corresponding conversion measurement without water in the feed (reductive conditions, see Table 1). The initial conversion rate for Fe_2O_3 is as high as with water in the feed and also the decrease is very similar. Post reaction characterization by AES (F in Tables 2 and 3) shows only carbon and not any signals from iron or oxygen. The carbon layer is so thick that it takes more than 10 TPO cycles before substrate signals start to reappear, in this case

Table 2

LEED patterns and intensity ratios of the main Auger peaks of carbon, oxygen, and iron before and after different treatments for the unpromoted Fe_2O_3 and Fe_3O_4 model catalysts

| Catalyst, treatment	LEED pattern	Phase from LEED	Auger intensity ratios		Label in Figs. 2, 3
			C/Fe	O/Fe	
Fe_2O_3 before reaction		Fe_2O_3	0	3.5	–
Fe_2O_3 after reaction with EB + H_2O		After 3 TPO cycles: Fe_3O_4	1.1 3.6 3.4	3.2 4.0 3.8	A B C
Fe_3O_4 before reaction		Fe_3O_4	0.0	2.9	–
Fe_3O_4 after reaction with EB + H_2O		After 4 TPO cycles: Fe_3O_4, disordered	5.0	3.5	D
Fe_2O_3 after reaction with EB	No pattern		5.3 ∞[a]	2.0 –	E F
Fe_2O_3 after reaction with EB + H_2O + O_2		After 1 TPO cycle: Fe_2O_3, disordered	0.8	3.4	G

[a] Only carbon visible in AES.
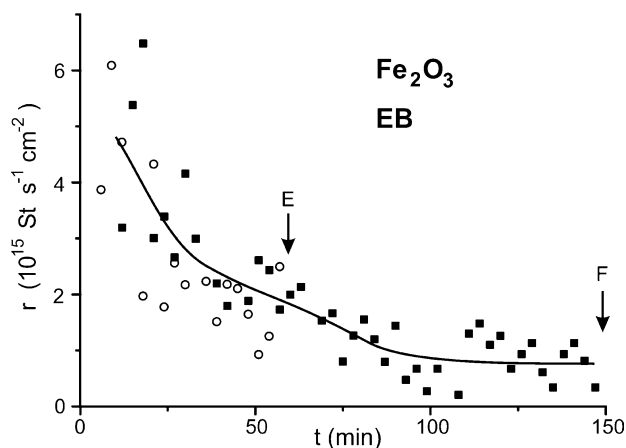
Fig. 3. Time dependence of the St conversion rate at 870 K over α-Fe_2O_3(0001) under reductive conditions (EB without H_2O in the feed).

from Pt. No LEED pattern of any of the iron oxide phases is seen. Instead, the pattern of the Pt(111) substrate is visible. Since a closed α-Fe_2O_3(0001) film reappeared after reoxidation, iron was obviously not lost but was reduced to Fe^0 and formed metallic clusters or had alloyed with the Pt substrate. The reaction was repeated on a freshly prepared catalyst and interrupted after 50 min (E in Fig. 3 and Table 2). AES shows

a strong decrease in the I_O/I_{Fe} ratio from 3.5 to 2.0 and strong coking $I_C/I_{Fe} = 5.3$.

Comparison of EB dehydrogenation with and without steam reveals the role of water in the reaction. Since the initial rate in both cases is the same, water is obviously not involved in the rate-determining step of the reaction. However, it prevents the pileup of carbon deposits and limits the reduction of the Fe_2O_3 to Fe_3O_4. This agrees with experiments on powder catalysts [3–8,13] and with thermodynamics [25].
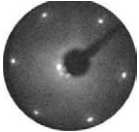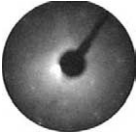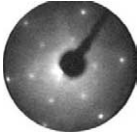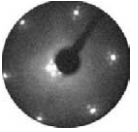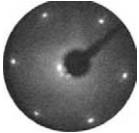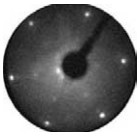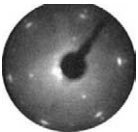
Also the final rate is the same in both cases. Since the surface in the case of reaction without water was completely covered by carbon, we believe that the final rate of $\sim 0.5 \times 10^{15}$ is characteristic for catalysis by carbon deposits.

3.1.3. Dehydrogenation on α-Fe_2O_3(0001) in the presence of steam and oxygen

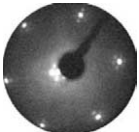Fig. 4a shows the conversion rate for St on unpromoted Fe_2O_3 after dosing oxygen to the feed (oxidative conditions, see Table 1). The initial high rate $\sim 6 \times 10^{15}$ can be maintained and no significant deactivation with time is observed. Postreaction characterization shows that the surface is almost free of carbon, $I_C/I_{Fe} = 0.8$, and the I_O/I_{Fe} ratio is not changed. After TPO, LEED shows that the film consists of unreduced α-Fe_2O_3(0001). However, the high background and broadness of the spots indicate a high defect concentra-

Table 3
LEED patterns and intensity ratios of the main Auger peaks of potassium, oxygen, carbon, and iron before and after different treatments for the promoted KFe_xO_y model catalysts

KFe_xO_y catalyst treatment		Auger intensity ratios			LEED patterns	
		K/Fe[a]	O/Fe	C/Fe	Before	After
(A) EB + H_2O	Before reaction	2.2	3.0	0		
	After reaction	1.9	2.8	2.1		
(B) EB + H_2O	Before reaction	0.9	2.3	0.0		
	After reaction	0.7	2.7	3.0		
(C) EB + H_2O	Before reaction	2.3	2.7	0		Not measured
	After reaction	1.8	2.5	0.5		
(D) After reaction and 15 min in H_2O EB + H_2O	Before reaction	[b]	[b]	[b]	Not measured	
	After reaction	0.6	2.6	4.4		
(E) EB + H_2O	Before H_2O treatment	2.8	2.7	0.0		Not measured
	After 15 min in H_2O	1.2	2.9	0.0		
(F) EB + H_2O + O_2	Before reaction	1.0	2.0	0.0		
	After reaction	0.90	1.9	0.6		

[a] I_K/I_{Fe} measured after TPO (for the separation of K from C).
[b] No AES measurement after reactivation.

tion (G in Table 2). The experiment was repeated and the oxygen concentration varied. The dependence of the steady-state rate on O_2 concentration (after an equilibration time of ~ 60 min) is shown in Fig. 4b.

Admission of oxygen prevents the reduction of Fe_2O_3 to Fe_3O_4 by consuming the H_2 produced during the dehydrogenation reaction or by reoxidizing the catalyst surface. It also burns off carbon deposits formed during reaction. Addition of higher O_2 concentrations (O_2:EB $\geqslant 1$) causes a considerable increase of total oxidation of EB.

3.2. Promoted iron oxide KFe_xO_y model catalyst

3.2.1. Dehydrogenation on KFe_xO_y in presence of steam and the effect of potassium content

Fig. 5a shows the conversion rate on a KFe_xO_y catalyst with $I_K/I_{Fe} = 2.2$, a K content slightly lower than for the K-β''-ferrite with ordered 2×2 surface. The initial conversion rate is the same as on unpromoted Fe_2O_3 shown for comparison, but deactivation is much slower and postreaction characterization after 4 h on stream shows less coke ($I_C/I_{Fe} = 2.1$, A in Table 3). After coke removal by TPO, AES reveals a moderate decrease in the potassium content to $I_K/I_{Fe} = 1.9$. Since the composition within the catalyst film equilibrates quickly at reaction temperature, this decrease represents K depletion in the whole film and is observable only because of the limited amount of potassium in the thin film catalyst. LEED after TPO cycles shows the same quasi-1×1 pattern as before reaction, but the spots are very weak and the background high, indicating a high defect concentration.

When the initial K content is lower ($I_K/I_{Fe} = 0.9$, Fig. 5b, B in Table 3) the starting conversion rate is higher but the deactivation rate is faster. AES after reaction shows more carbon deposits ($I_C/I_{Fe} = 3.0$) and a similar moderate decrease in the potassium content to $I_K/I_{Fe} = 0.7$.
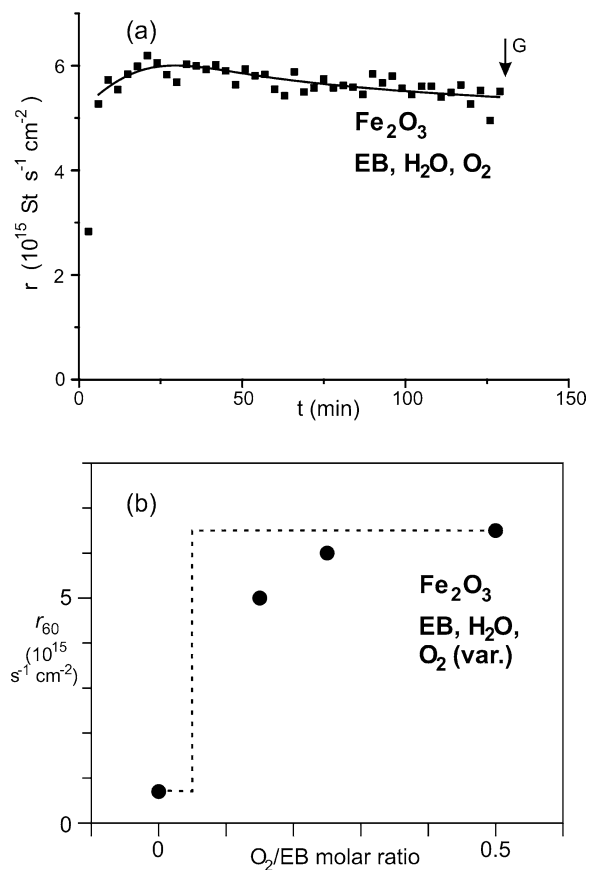
Fig. 4. (a) Time dependence of the St conversion rate at 870 K over α-Fe_2O_3(0001) under oxidative conditions (EB, H_2O, and O_2 in the feed). (b) Dependence of the steady-state rate r_{60} after 60 min reaction on the O_2 concentration it terms of the O_2:EB molar ratio.

Fig. 5. Time dependence of the St conversion rate at 870 K over KFe_xO_y, normal conditions, EB and H_2O in the feed. (a) $I_K/I_{Fe} = 2.2$; comparison: Fe_2O_3 as in Fig. 2a. (b) $I_K/I_{Fe} = 0.9$.

In Fig. 6, the accumulation of carbon deposits during reaction is compared for an unpromoted and a promoted catalyst with relatively high K content ($I_K/I_{Fe} = 2.8$). The experiment was interrupted at different times for AES measurements and continued afterward. The steady-state level on the promoted catalyst is lower and only reached after a longer time on stream. Postreaction characterization after TPO again shows a loss of potassium ($I_K/I_{Fe} = 1.8$). This confirms the role of potassium in preventing or removing carbon deposits, thus slowing down deactivation by coking. It has been proposed that coke is removed in a reaction cycle in which oxidic K and H_2O form KOH which reacts further with carbon to form K_2CO_3. The carbonate decomposes, releases CO_2, and leaves K-oxides behind [7,8,11,12].

3.2.2. The effect of steaming KFe_xO_y catalysts

In the industrial process, a deactivated catalyst is reactivated by running the reactor with steam only in the feed. Fig. 7a shows the conversion rate on KFe_xO_y catalyst with a similar K content as in Fig. 5a ($I_K/I_{Fe} = 2.3$). After reaction, the carbon deposits are low $I_C/I_{Fe} = 0.5$ and the potassium content has moderately decreased to $I_K/I_{Fe} = 1.8$ (C in Table 3). After characterization, the catalyst was transferred back to the reactor and the experiment was continued for

Fig. 6. Time dependence of carbon buildup over unpromoted Fe_2O_3 and potassium-promoted KFe_xO_y, $I_K/I_{Fe} = 2.8$.

15 min with only water and no EB in the feed gas. Then the normal EB flux was introduced again and the rate measured. Fig. 7b shows that the initial conversion rate is now higher, but the deactivation rate is faster. Postreaction characterization with AES shows strong coking ($I_C/I_{Fe} = 4.4$). Both the

Fig. 8. Time dependence of the St conversion rate at 870 K, oxidative conditions (EB, H_2O, and O_2 in the feed) over KFe_xO_y ($I_K/I_{Fe} = 1.0$).
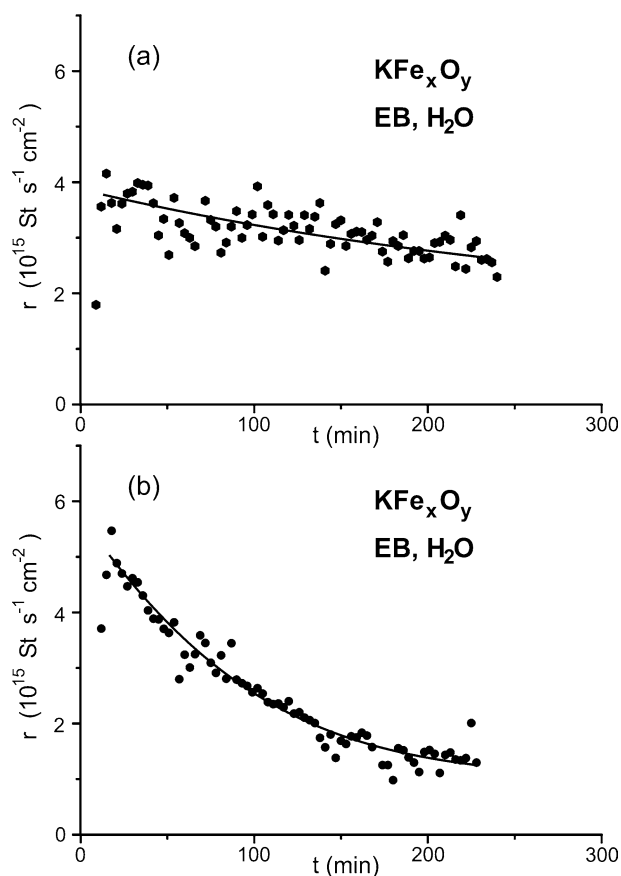
Fig. 7. Time dependence of the St conversion rate at 870 K, normal conditions, EB and H_2O in the feed, over (a) KFe_xO_y ($I_K/I_{Fe} = 2.2$). (b) After 15 min of reactivation in H_2O without EB.

increased initial conversion rate and the faster deactivation are characteristic for a catalyst with low initial K content like that of Fig. 5b (B in Table 3). In fact, AES after TPO shows a strongly decreased potassium content $I_K/I_{Fe} = 0.6$ (D in Table 3). In order to substantiate further that enhanced K loss is caused by "regeneration" in steam, a clean promoted catalyst ($I_K/I_{Fe} = 2.8$) was analyzed with AES analysis directly before and after the corresponding steam treatment. The data (E in Table 3) confirm clearly that K loss during steaming is faster than in the presence of EB and its reaction products.

The continuous decrease of the K content during reaction, the enhanced depletion by steaming, and the faster deactivation for samples with lower K content prove that the loss of potassium from the active near-surface region is the major reason for the decay of the long-term catalytic activity as pointed out in studies on real catalysts [9]. In real catalyst pellets, phase separation into a deep lying K-rich phase not accessible for the reactants and a K-depleted outer shell was identified as one deactivation process. This cannot be simulated in our thin film model catalysts. As a second path for K-depletion, removal in form of gaseous KOH was proposed [11]. KOH has a vapor pressure of about 0.1 mbar at
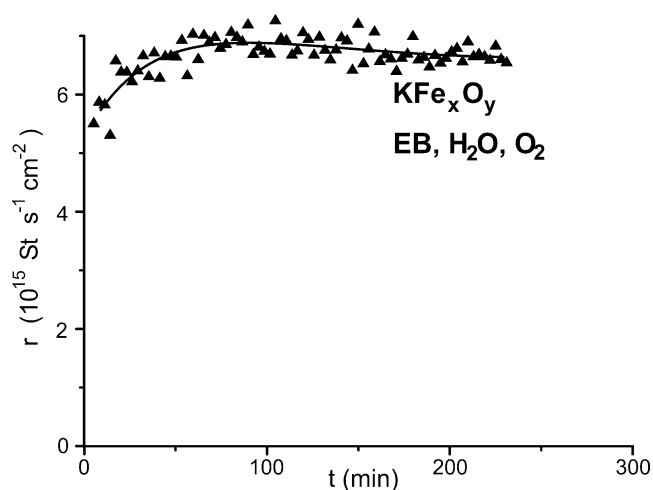
the reaction temperature. This is the likely mechanism of removal in our studies.

In order to check the removal of carbon deposits by steaming, the corresponding 15-min treatment in water was repeated on a carbon-covered promoted catalyst. In fact, AES after steaming shows not any carbon deposits. Thus, steaming removes coke [4,6–8] but this is accompanied by the removal of nonnegligible amounts of potassium from the catalyst's potassium reservoir. Therefore, the overall lifetime of the catalyst is appreciately decreased by each steaming treatment.

From the fact that K loss is slower in presence of EB and its reaction products, we conclude that carbon must be involved in the formation of a protection layer. This could be a thin layer of carbonaceous deposits but we consider it more likely that a potassium containing species with lower vapor pressure is formed. A candidate is again the carbonate K_2CO_3 [7,8]. As described above, the presence of coke opens the possibility of KOH to form carbonate instead of evaporating thus decreasing the rate of K removal.

3.2.3. Dehydrogenation on KFe_xO_y in presence of steam and oxygen

The influence of adding oxygen to the feed (oxidative conditions, Table 1) on the conversion rate and the deactivation behavior is presented in Fig. 8 for a catalyst with a fairly low K content, $I_K/I_{Fe} = 1.0$. The initial conversion is high, increases slightly to the highest value observed so far, and remains on this level. The behavior is similar to that of the unpromoted catalyst in presence of O_2 (Fig. 4a). AES after reaction indicates only a small loss of potassium, only a small amount of carbon deposits $I_C/I_{Fe} = 0.6$, and an almost unchanged I_O/I_{Fe} ratio (F in Table 3). It seems that O_2 not only supports removal of coke but also stabilizes the potassium, possibly by stabilizing a K_2CO_3 coverage layer. LEED after TPO shows that the film still exhibits the same

quasi-1×1 pattern but also here, the enhanced background indicates an increased defect concentration.

3.2.4. Dehydrogenation on KFe_xO_y without steam

The reaction under reductive conditions (Table 2) with only EB (and He) in the feed was run on a promoted catalyst with $I_K/I_{Fe} = 1.2$ and $I_O/I_{Fe} = 2.5$. Surface characterization by AES after 45 min showed the usual K decrease ($I_K/I_{Fe} = 0.8$) and a moderate coke deposition ($I_C/I_{Fe} = 0.7$) but almost no decrease of I_O/I_{Fe}. In contrast, O depletion was clear on the unpromoted catalyst (E in Table 2). This demonstrates that the potassium promoter in fact prevents reduction of the iron oxide, possibly by strengthening the Fe–O bond [8,10,26]. The conversion does not decrease quickly or dramatically when the water in the feed is stopped after some hours from reaction in EB and water. This supports the interpretation that deactivation goes along with K depletion while coking anyway is not a serious problem on the promoted catalyst, at least on the relatively short time scale investigated here.

4. Discussion

The approach using pore-free thin single crystalline films as model catalysts rules out uncertainties due to transport of matter within the catalyst material like pore diffusion, pore filling by coke, and influence of catalyst shaping on the activity. Due to the perfect heat contact to the metallic carrier of the thin films, also temperature inhomogeneities do not exist and the existence of hot spots, etc., is ruled out. Within the thin films, kinetic limitations of solid-state chemical processes are less important, and at the reaction temperature compositional changes caused by surface reactions are quickly equilibrated. This and the limited amount of matter in the films results in a clear assignment of catalyst composition, phase and structure to its activity. The stagnation point arrangement is well defined and allows modeling which will be the subject of future work.

4.1. Unpromoted model catalysts

The reactivity measurements in connection with pre- and postcharacterization on the unpromoted Fe_2O_3 catalyst showed that the initial conversion rate is high and that deactivation is due to reduction of Fe_2O_3 to Fe_3O_4 and to coking. The high initial activity is related to clean Fe_2O_3 while the activity of clean Fe_3O_4 is lower. Especially since the addition of oxygen stabilizes the high initial activity, it is important to check if it is the oxygen liberated during substrate reduction which is responsible for the high starting rate on Fe_2O_3. Lattice oxygen could be consumed by the hydrogen produced from the EB dehydrogenation to form water according to the equation

$$C_8H_{10} + 3Fe_2O_3 \rightarrow C_8H_8 + 2Fe_3O_4 + H_2O. \tag{3}$$

This would be a simple stoichiometric reaction which could be prevented by admission of O_2

$$2Fe_3O_4 + \tfrac{1}{2}O_2 \rightarrow 3Fe_2O_3. \tag{4}$$

Since our starting films are about 10–20 nm thick, a simple estimation yields the amount of O_2 liberated when the whole film is reduced to Fe_3O_4. Comparison with the amount of styrene formed (which equals the amount of formed H_2) within the high rate region in Fig. 2a ($\sim$ 15 min with rate of 4×10^{15} molecules s^{-1} cm^{-2}) shows that styrene production is at least by a factor of 700 higher. The dehydrogenation reaction of ethylbenzene to styrene over clean Fe_2O_3 is thus essentially catalytic. The stoichiometric reaction (3) may be a side reaction.

The equilibrium thermodynamics of the Fe–O_2–H_2–H_2O system has been investigated experimentally by Muan [25]. For the reaction temperature of 870 K, Fe_2O_3 is reduced in presence of H_2. Without H_2O, this proceeds to metallic Fe^0 while the presence of H_2O limits reduction to Fe_3O_4. The hydrogen produced during EB dehydrogenation is thus responsible for the observed reduction effects. This agrees well with recent reduction experiments by Ndlela and Shanks [10]. The role of H_2O is not only to balance coke formation by the coal gasification reaction but also to limit reduction beyond the magnetite (Fe_3O_4) phase.

Thermodynamic considerations showed also that hematite (Fe_2O_3) reduction can be prevented by addition of oxygen. The necessary minimum amount corresponds almost to that necessary for the stoichiometric water formation reaction $H_2 + \tfrac{1}{2}O_2 \rightarrow H_2O$. The high conversion rate observed with O_2 in the feed (Fig. 4a) corresponds to a conversion of about 10% of the introduced EB. The formed $p(H_2)$ would thus correspond to 10% of $p(EB)$. The necessary oxygen for its oxidation would be 5% of $p(EB)$ and a molar ratio above O_2:EB $= 0.05$ should be sufficient to prevent Fe_2O_3 reduction. If thermodynamic equilibrium would be established, the dashed step curve in Fig. 4b would be expected for the dependence of the steady-state rate on the O_2:EB ratio. The measured steady-state rates show a reduction with respect to the standard oxygen concentration O_2:EB $= 0.5$ by about 10% for O_2:EB $= 0.25$ and by 25% for O_2:EB $= 0.15$.

There may be two reasons for the rate decay before reaching the theoretical limit of O_2:EB $= 0.05$. Thermodynamic equilibrium may not to be established within the reactor or a part of the oxygen may be consumed for the oxidation of coke. Each EB molecule, which is converted into partially dehydrogenated species or graphitic coke and hydrogen, needs 10.5 or 6.5 O_2 molecules for oxidation of all formed products into H_2O and CO_2 or CO, respectively (total oxidation):

$$C_8H_{10} + 10\tfrac{1}{2}O_2 \rightarrow 8CO_2 + 5H_2O, \tag{5}$$

$$C_8H_{10} + 6\tfrac{1}{2}O_2 \rightarrow 8CO + 5H_2O. \tag{6}$$
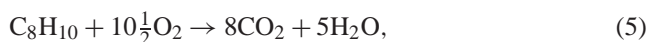
In the presented experiments, about 5% of the introduced EB did not show up as aromatics in the GC measurements.

This represents the upper limit of EB consumed for coking and a flow ratio $O_2:EB = 0.525$ [reaction (5)] or 0.325 [reaction (6)] would be necessary to oxidize it continuously. One might think that less oxygen may be necessary since the coke is also partially removed by the water in the feed by the coal gasification reaction. Including the hydrogen formed during dehydrogenation in the coking process, this leads to the sum reaction

$$C_8H_{10} + 16H_2O \rightarrow 8CO_2 + 21H_2 \qquad (7)$$

or

$$C_8H_{10} + 8H_2O \rightarrow 8CO + 13H_2. \qquad (8)$$
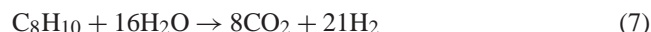
In order to prevent catalyst reduction, it is necessary to oxidize all the produced H_2. The necessary amounts of O_2 correspond to $O_2:EB = 0.525$ and 0.325, respectively, for Eqs. (7) and (8) and are, of course, the same as without the influence of water. It thus turns out that oxidation of coke and of the hydrogen liberated during coking dominates the necessary amount of oxygen to be added. The estimation shows further that the experimentally applied oxygen flow for a maximum rate ($EB:O_2 = 1:0.5$) is near to the optimal level.

The observed reduction of the hematite to magnetite agrees with observations on technical catalysts [9,16]. However, the high initial rate associated with clean hematite was not observed before. Obviously it was hidden in the start-up and equilibration period. It is therefore likely that only the fully deactivated state was observed in the investigations on technical catalysts. An exception is a recent measurement on pressed Fe_2O_3 powder pellets under technical conditions (1 bar, pure $EB + H_2O$ atmosphere, $EB:H_2O = 1:6$) where the initial high conversion rate decreased within the first minutes on stream by a factor of $\sim 8–10$ [27]. Upon addition of oxygen ($EB:H_2O:O_2 = 1:6:0.4$), the steady-state conversion did not rise to the initial value but could at least be enhanced by a factor of three. The concentration of O_2 was obviously not sufficient for full prevention of reduction and coking. The conversion rate (referred to the BET surface) on the powder catalyst was about two orders of magnitude lower than on the model catalyst which indicates that it is limited by mass and energy transport on the powder catalyst.

In low and medium pressure experiments $p(EB) + p(H_2O) = 3.5 \times 10^{-6}$ [15] to 0.6 mbar [14] there was clear evidence that defective Fe_2O_3 surfaces are catalytically more active than well-ordered ones. In the high-pressure experiments presented here, [$p(EB) + p(H_2O) = 36$ mbar], no indications for a defect-dependent initial activity was observed, but postreaction analysis showed always that disorder had formed during reaction. Formation of disorder is plausible because of the observed reduction which implies out-diffusion of oxygen and nucleation of magnetite with its different crystal structure. While at low and medium pressures the formation of defects is slow enough so that the influence of initial surface disorder is clearly visible, the
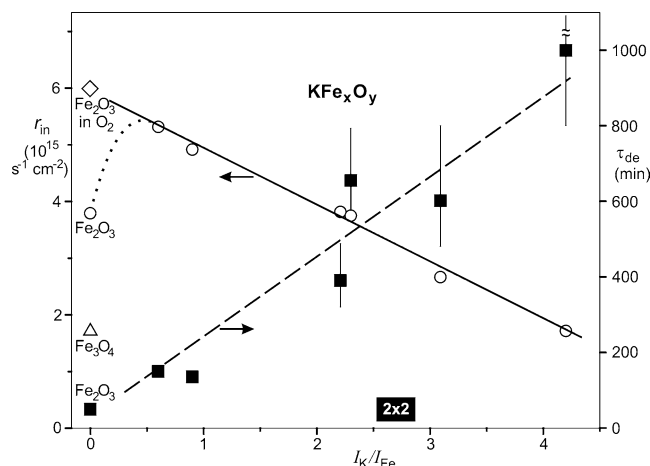

Fig. 9. Dependence of the initial conversion rates r_{in} and the time constant of deactivation τ_{de} on the K content in terms of I_K/I_{Fe}. The initial rates for unpromoted samples for normal and oxidative conditions are included.

more violent reaction conditions at high pressure may accelerate defect formation so that it has happened within the first minutes and may at most influence the first GC data point after gas admission. The importance of defects for the mechanism of the catalytic reaction could thus only be deduced from low-pressure experiments.

The final activity after deactivation is definitely not zero. We have presented strong evidence that it can be ascribed to carbonaceous deposits. It is well known that certain forms of carbon are active catalysts in oxidative dehydrogenation of EB [28,29]. If no oxygen is added and after reduction of the substrate, the only source of oxygen is the water which may supply oxygen according to the dissociation equilibrium at the reaction temperature or to the coal gasification reaction which may supply CO. Postreaction Auger analysis also revealed oxygen at the surface in this case. When no water is added, even this source of oxygen is lacking. Consequently, no oxygen was visible in AES. However, the final activity in Figs. 2a and 3 was the same, independent of the presence of water. The mechanism over the deactivated catalyst is thus not yet clear.

4.2. K-promoted model catalysts

Conversion measurements were run over several model catalysts with different initial K content. Fig. 9 summarizes the dependence of the initial conversion rates r_{in} and of the time constant of deactivation τ_{de} on the K content in terms of I_K/I_{Fe}. Also the initial rates for the unpromoted samples (Fe_2O_3, Fe_2O_3, Fe_2O_3 with O_2 added to the feed) are included. The initial rate decreases and the time constant for deactivation (assuming an exponential decay of the rates) increases with the K content. A simple explanation of this behavior would be that K prevents catalyst deactivation by reduction and coking but at the same time reduces or blocks active surface sites. For $I_K/I_{Fe} > 2.7$, the surface is increasingly covered by $KFeO_2$ [22,23]. The further decrease of the

rate in this range suggests that $KFeO_2$ is not the catalytically active phase. However, its presence may be responsible for slow deactivation.

For low K content, the initial rate in Fig. 9 tends toward the rate of Fe_2O_3 with O_2 in the feed while the rate of Fe_2O_3 without O_2 is lower (dotted curve). We believe that this is caused by partial deactivation of Fe_2O_3 before the first data point of the rate curve (Fig. 2a) can be taken. It is plausible to assume that the topmost surface layer is partially reduced quite quickly so that the rate approaches that of Fe_3O_4 while addition of O_2 prevents this.

With oxygen in the feed, the reaction rates on the unpromoted (Fig. 4a) and on the promoted catalyst (Fig. 8) are very similar concerning both their magnitude and their time dependence. It seems therefore feasible to use oxygen in the feed instead of promotion by potassium.

All results point toward the direction that potassium prevents coking and catalyst reduction but does not directly take part in the catalytic reaction. Since the initial activity on unpromoted Fe_2O_3 and on promoted films (I_K/I_{Fe} between 2.2 and 3) is quite similar (Fig. 5a), it suggests that the active sites and mechanisms are the same and are related to Fe^{3+} without the presence of Fe^{2+} in the proximity. Because of not too different apparent activation energies, this has already been proposed for polycrystalline catalysts [6]. However, in that case the activity of the unpromoted catalyst was an order of magnitude lower than for the promoted catalyst. According to the model catalysis results reviewed here, this means that the unpromoted catalyst was most likely deactivated, i.e., reduced and coked.

Also the addition of oxygen does not change the initial activity dramatically. The mechanism of the main reaction path may therefore not either be influenced by the presence of oxygen. It is not oxidative in the sense that oxygen takes part directly in the catalytic reaction. It rather balances the effects of catalyst reduction by the hydrogen formed in the catalytic reaction and during coking, both being side reactions of the process. And it oxidizes the deposited carbon.

The active site requires Fe^{3+} but the Fe^{3+} in Fe_3O_4 is obviously not equally active. It could be that a pure Fe^{3+} environment is necessary as present in Fe_2O_3, in $KFeO_2$, and formally also in $K_2Fe_{22}O_{34}$. An alternative explanation was discussed by Kuhrs et al. [30] on the basis of the binding energies of EB and St to the different model catalyst surfaces. Due to the existence of iron in the top layer of Fe_3O_4, EB and even more St are bound strongly and may block the surface under reaction conditions while bonding to Fe_2O_3 and $K_xFe_{22}O_{34}$ is much weaker and more similar for EB and St. In hematite, the first layer consists of oxygen, possibly hydroxylated [31] and in K-β''-ferrite, it is most likely formed by K and O [22]. These layers separate the adsorbate from the Fe layer below but the distance is small enough to let the adsorbate still feel the acidic character of the Fe^{3+} sites underneath. The interaction with Fe_2O_3 and $K_xFe_{22}O_{34}$ is sufficient to bind the EB molecule long enough to the surface to enable dehydrogenation but neither EB nor St so strongly

that they block the surface. This is an example of the old wisdom in catalysis that the bond should be strong enough but not too strong.

Based on the observations that both the right adsorption strength and—at least on unpromoted Fe_2O_3—defects are necessary for high conversion, a model for the catalytic cycle has been proposed [32]. The adsorbate–substrate bond via the π-system of the benzene ring is responsible for holding the molecules long enough on the surface. Probably, they are mobile at the reaction temperature and move over the surface until they meet a defect site exposing basic oxygen which attracts the H atoms of the ethyl group and dehydrogenates it. Simultaneously, two Fe^{3+} ions in the vicinity are formally reduced to Fe^{2+} which explains why Fe^{3+} is necessary and why iron with its variable valency is essential. The formed styrene desorbs. The mechanism of H removal from the catalyst and reoxidation of Fe^{2+} is speculative. However, the presented results suggest that a direct desorption in the form of H_2 is possible. In the main reaction path, it does not seem to be removed as H_2O by consuming substrate oxygen which later would have to be replaced by dissociation of water or by reaction with O_2 from the feed (Mars–Van Krevelen mechanism). Substrate oxygen is consumed but this is only a side reaction and leads to reduction of the substrate to Fe_3O_4 which is irreversible when only H_2O and no O_2 is added to the feed.

So far, nothing is known about the structure of the anticipated protection layer against K removal on the promoted catalyst which possibly consists of K carbonate. Since the "protection" has to be effective for K only, it could be that the local structure of the active sites consists of O above Fe^{3+}, an arrangement similar to that on Fe_2O_3. Maybe, surface K carries a carbonate group, maybe by inclusion of surface O.

In the literature, it was found that the presence of $KFeO_2$ is necessary for high and long-term activity. Therefore it was proposed that it represents the catalytically active surface phase on promoted catalysts while K-β''-ferrite $K_2Fe_{22}O_{34}$ was supposed to be the bulk phase below, representing a K-reservoir for the reestablishment of $KFeO_2$ [7,8]. Previous studies on model catalyst preparation [22,23] indeed showed that $KFeO_2$ forms when a layer of K deposited on Fe_3O_4 is annealed at 700 K. Annealing to the reaction temperature 870 K results in a thin $KFeO_2$ layer or $KFeO_2$ islands on K-β''-ferrite and at 970 K, no $KFeO_2$ is left. The surface is then terminated by a full Fe–O–K layer forming an ordered 2×2 superstructure in LEED. Since surface and bulk composition equilibrate quickly at temperatures above about 600 K [22], this surface layer can only be established when the bulk contains an amount of K which corresponds at least to substoichiometric $K_xFe_{22}O_{34}$ ($x \geqslant 0.67$). The K-promoted films in our study with $2 < I_K/I_{Fe} < 2.5$ surely consisted only of K-β''-ferrite without any $KFeO_2$ on the surface. Nevertheless, they deactivate slowly and have a high conversion rate (Figs. 4a and 6a). $KFeO_2$ which forms on the surface for $I_K/I_{Fe} > 2.7$ causes the initial rate to decrease

further thus ruling out that it is the catalytically most active phase. However, the deactivation proceeds even more slowly. It is thus likely that the role of active phase and reservoir phase is inverted; i.e., K-β''-ferrite is the active phase and $KFeO_2$ represents the K reservoir. Intuitively this seems plausible. The coincidence of long-lasting high activity with the presence of the $KFeO_2$ phase does not necessarily mean that it is the active phase. It could be as well that the reservoir phase is necessary to guarantee at least the substoichiometric of K-β''-ferrite with Fe–O–K termination while the stoichiometry and the surface K content drops when the reservoir phase is consumed. The existence of $KFeO_2$ would thus "buffer" the K-β''-ferrite phase against K-depletion by reaction with H_2O, an interpretation which is in full agreement with the experimental findings in [7,8].

5. Conclusions

The pressure and material gap between reactivity studies in UHV and real catalysis can only be overcome by application of in situ methods of catalyst characterization and activity measurements under realistic pressure and temperature conditions as has been done in this study. Well-defined thin epitaxial films of the compositions $Fe_3O_4(111)$, α-$Fe_2O_3(0001)$, $K_xFe_{22}O_{34}$ ($x \leqslant 0.67$) and $KFeO_2$ were prepared, transferred into a stagnation point microflow reactor for conversion measurements and afterward transferred back for postreaction surface characterization.

The initial conversion rates on unpromoted and K-promoted catalysts are similar. On unpromoted Fe_2O_3, deactivation is fast and is caused both by reduction to Fe_3O_4 and by coking. Water added to the reactant seems not to be involved in the main catalytic reaction. As proposed before, it is essential for gasification of carbon deposits thus limiting its amount. Further it limits reduction of the iron oxide to the oxidation state of Fe_3O_4 and prevents further reduction to metallic iron. The high initial conversion of Fe_2O_3 can be maintained by adding a small amount of oxygen to the feed. This prevents reduction and keeps carbon deposits at a low level. The main dehydrogenation path is a simple catalytic reaction. There is no indication for a Mars–Van Krevelen mechanism.

Potassium as promoter reduces the buildup of carbonaceous deposits and prevents reduction of the oxide. The initial conversion rate decreases with increasing potassium loading, which is explainable by blocking of active sites by excess potassium. However, high potassium contents lead to slower deactivation by coking. $KFeO_2$ is not the active phase but serves as K reservoir. Potassium is continuously removed during reaction, most likely in form of volatile KOH. The removal rate is considerably faster if the feed contains only water and no EB. It is suggested that EB, St, or their decomposition products react with potassium to form carbonate. "Steaming" the catalyst should thus be avoided. Oxidation in O_2 could be an alternative. Also on the promoted catalyst,

it was possible to maintain a high activity by the addition of oxygen. Addition of oxygen appears favorable and could even replace promotion by potassium. Because of the presence of hydrogen, a technical realization depends on the possibility to control security questions.

Evidence is given that the existence of Fe^{3+} is not sufficient for high activity. The adsorption strength for EB and St is essential as well. The lower conversion on Fe_3O_4 relates with its higher adsorption strength which may lead to site blocking.

References

[1] K. Kochloefl, in: G. Ertl, H. Knözinger, J. Weitkamp (Eds.), Handbook of Heterogeneous Catalysis, vol. 5, VCH, Weinheim, 1998, p. 2151.
[2] Nova Chemicals Corp., www.novachem.com/investorrelations/reports/2000AnnualReport/FactBook2000.pdf, Supplemental Financial and Product Information 2000, 2000.
[3] E.H. Lee, Catal. Rev. 8 (1973) 285.
[4] T. Hirano, Appl. Catal. 26 (1986) 65.
[5] T. Hirano, Appl. Catal. 28 (1986) 119.
[6] K. Coulter, D.W. Goodman, R.G. Moore, Catal. Lett. 31 (1995) 1.
[7] M. Muhler, J. Schütze, M. Wesemann, T. Rayment, A. Dent, R. Schlögl, G. Ertl, J. Catal. 126 (1990) 339.
[8] M. Muhler, R. Schlögl, G. Ertl, J. Catal. 138 (1992) 413.
[9] J. Matsui, T. Sodesawa, F. Nozaki, Appl. Catal. 51 (1989) 203.
[10] S.C. Ndlela, B.H. Shanks, Ind. Eng. Chem. Res. 42 (2003) 2112.
[11] W.D. Mross, Catal. Rev.-Sci. Eng. 24 (1983) 591.
[12] R.L. Hirsch, J.E. Gallagher, R.R. Lessard, R.D. Wesselhoft, Science 215 (1982) 121.
[13] W.P. Addiego, C.A. Estrada, D.W. Goodman, M.P. Rosynek, R.G. Windham, J. Catal. 146 (1994) 407.
[14] W. Weiss, D. Zscherpel, R. Schlögl, Catal. Lett. 52 (1998) 215.
[15] D. Zscherpel, Adsorption und Dehydrierung von Ethylbenzol auf epitaktischen Eisenoxidfilmen, in: Forschungsberichte Physik, vol. 9, Oberhofer, Berlin, 1999.
[16] G.R. Meima, P.G. Menon, Appl. Catal. A 212 (2001) 239.
[17] F. Cavani, F. Trifiro, Appl. Catal. A 133 (1995) 219.
[18] W. Weiss, W. Ranke, Progr. Surf. Sci. 70 (2002) 1.
[19] C. Kuhrs, M. Swoboda, W. Weiss, Top. Catal. 15 (2001) 13.
[20] G. Ketteler, W. Weiss, W. Ranke, R. Schlögl, Phys. Chem. Chem. Phys. 3 (2001) 1114.
[21] S.K. Shaikhutdinov, W. Weiss, Surf. Sci. 432 (1999) L627.
[22] Y. Joseph, G. Ketteler, C. Kuhrs, W. Ranke, W. Weiss, R. Schlögl, Phys. Chem. Chem. Phys. 3 (2001) 4141.
[23] G. Ketteler, W. Ranke, R. Schlögl, J. Catal. 212 (2002) 104.
[24] W. Ranke, W. Weiss, Surf. Sci. 465 (2000) 317.
[25] A. Muan, Am. J. Sci. 256 (1958) 171.
[26] D.E. Stobbe, F.R. VanBuren, A.J. VanDillen, J.W. Geus, J. Catal. 135 (1992) 533.
[27] O. Shekhah, W. Ranke, A. Schüle, G. Kolios, R. Schlögl, Angew. Chem. Int. Ed. 42 (2003) 5760.

[28] G. Mestl, N.I. Maksimova, N. Keller, V.V. Roddatis, R. Schlögl, Angew. Chem. Int. Ed. 40 (2001) 2066.

[29] N. Keller, N.I. Maksimova, V.V. Roddatis, M. Schur, G. Mestl, Y.V. Butenko, V.L. Kuznetsov, R. Schlögl, Angew. Chem. Int. Ed. 41 (2002) 1885.

[30] C. Kuhrs, Y. Arita, W. Weiss, W. Ranke, R. Schlögl, Top. Catal. 14 (2001) 111.

[31] G. Ketteler, W. Weiss, W. Ranke, Surf. Rev. Lett. 8 (2001) 661.

[32] Y. Joseph, M. Wühn, A. Niklewski, W. Ranke, W. Weiss, C. Wöll, R. Schlögl, Phys. Chem. Chem. Phys. 2 (2000) 5314.